



CLICdp-Note-2018-007
26 September 2019

A DELPHES card for the CLIC detector

E. Leogrande*, P. Roloff*, U. Schnoor¹⁾*, M. Weber*

* CERN, Switzerland

Abstract

The Compact Linear Collider, CLIC, is a multi-TeV electron-positron collider proposed for construction at CERN. A detector model, CLICdet, that is suited for the experimental conditions at CLIC and is based on realistic performance, has been developed. This paper describes the implementation of CLICdet in a fast simulation tool for particle physics collider experiments, DELPHES. The geometry of the detector concept as well as performance parameters extracted from full simulation studies are implemented in DELPHES parameter cards for CLICdet. Jet reconstruction for electron-positron colliders is added to the DELPHES analysis chain. Parameters for using DELPHES to simulate the detector effects of CLICdet are provided in three parameter cards, one for each energy stage of CLIC. The effects of beam-induced background at the higher-energy stages of CLIC are also incorporated. The results from the fast simulation with DELPHES are validated with respect to full detector simulation in a number of relevant processes.

This work was carried out in the framework of the CLICdp Collaboration

© 2019 CERN for the benefit of the CLICdp Collaboration.

Reproduction of this article or parts of it is allowed as specified in the CC-BY-4.0 license.

¹ulrike.schnoor@cern.ch

1. DELPHES for fast simulation of detector effects at CLIC

The detector model for CLIC, CLICdet, has been defined and described in [1] and its performance is discussed in detail in [2]. Full simulation collision events can be obtained by running the simulation and reconstruction chain on hadron-level Monte Carlo events generated e.g. with WHIZARD [3] and PYTHIA6 [4]. Such a full detector simulation is performed for signal and background events for most of the studies carried out in the framework of the CLICdp collaboration, e.g. [5, 6]. In order to optimise the design of the detector and to understand fully its impact on the proposed physics programme, the full detector simulation and event reconstruction framework is essential. However, for many studies including some of those of an exploratory nature or where the relative sensitivity to physics parameters is paramount, a faster simulation tool is extremely useful.

The fast simulation framework DELPHES [7–9] is a modular system which emulates the impact that the full detector simulation will have on hadron-level simulation of collision events. These include the effects of detector geometry, detector response and resolution as well as reconstruction performance of physics objects. It can be used to approximate those kinematic distributions for which the detector effects are well described by a parametrisation. The simulation with DELPHES requires much less CPU time than a full detector simulation which models the interactions of particles with the material of the detector. According to the specific detector, an input parameter card must be provided. This document describes the parameter card developed for the CLICdet detector model. It has been used for several studies carried out in the framework of the recent report on the CLIC potential for new physics [10].

A generic layout of a general-purpose detector for particle collider experiments is implemented in DELPHES, of which some geometry parameters can be modified according to the given detector model. In addition, the performance of identification and reconstruction based on certain objects and particle types can be defined in the detector card. The geometry and performance parameters inserted into the CLICdet card are described in Sec. 2. The order in which detector effects are applied to generator level objects is described in Sec. 3.1. Until recently, DELPHES has been used predominantly for studies at hadron colliders, in particular the LHC. Jet clustering at e^+e^- colliders offers additional features which have been implemented into the DELPHES framework in the context of the development of the parameter card. This is described in Sec. 3.2. Sec. 4 describes the validation of the DELPHES card, comparing its results for important physics processes with full detector simulation. Additional validation plots can be found in Appendix B. The parameter card has been merged into the central DELPHES repository and can be accessed at [11]. User instructions are given in Appendix A.

2. Performance parameters of the CLICdet detector

2.1. The CLICdet detector

The current detector model for CLIC, CLICdet, is adapted to the high-energy e^+e^- collision environment at CLIC and optimised for particle flow reconstruction. The CLICdet concept was developed based on the lessons learned from the previous detector models for CLIC: CLIC_ILD and CLIC_SiD [12].

The CLICdet model comprises a low-mass silicon vertex and tracking system with a central barrel and forward disks. CLICdet is optimised for particle flow in particular by using highly granular calorimetry based on silicon-tungsten electromagnetic calorimeters and scintillator-steel hadronic calorimeters. A superconducting solenoid surrounding the calorimeters provides a magnetic field of 4 T. Beyond the solenoid, an iron yoke is interleaved with muon chambers. In the forward region, close to the beam pipe, CLICdet contains two specialised forward electromagnetic calorimeters to measure luminosity and beam properties as well as to extend the acceptance.

The two previous models differ from CLICdet in the following main aspects[1]: The CLIC_SiD concept uses a 5 T magnetic field and a smaller radius tracking system. CLIC_ILD uses a TPC as tracking system. In both cases, tungsten is used as absorber in the barrel of the hadronic calorimeter.

While the CLIC DELPHES card is based on the CLICdet performance, some of the validation studies for which no CLICdet simulation was available are based on one of the previous detector concepts.

The right-handed coordinate system has its origin at the centre of the detector, the z axis along the detector axis close to the beam direction, and the y axis pointing upwards. While most studies of e^+e^- collisions employ the polar angle θ coordinate, defined with respect to the positive z axis, this note mainly uses the pseudorapidity as it is the standard for DELPHES. The pseudorapidity η is defined as $\eta = -\ln[\tan(\theta/2)]$ and the distance ΔR in the pseudorapidity-azimuth plane is defined as $\Delta R = \sqrt{\Delta\eta^2 + \Delta\phi^2}$.

Under the baseline staging scenario, CLIC is expected to deliver 1 ab^{-1} of luminosity at $\sqrt{s} = 380 \text{ GeV}$, 2.5 ab^{-1} at $\sqrt{s} = 1.5 \text{ TeV}$, and 5 ab^{-1} at $\sqrt{s} = 3 \text{ TeV}$ [13]. The luminosity will be shared evenly between an electron beam polarisation of $P(e^-) = -80\%$ and $+80\%$ at the first stage. At the higher energy stages, 80% (20%) of the luminosity will be collected with $P(e^-) = -80\%$ ($P(e^-) = +80\%$).

2.2. Performance parameters for the DELPHES card

The performance of CLICdet has been thoroughly evaluated using full detector simulation in [2]. The detector geometry of CLICdet for the full simulation is implemented within the DD4HEP framework [14] and simulated in GEANT4 [15–17]. The reconstruction software is implemented in the Linear Collider framework MARLIN [18]. Track reconstruction is performed with the Conformal Tracking method [19]. Based on the reconstructed tracks and calorimeter deposits, particle flow clustering is performed using PandoraPFA [20–22]. Flavour tagging is applied using the LCFIPLUS package [23].

Three cards for the three energy stages of CLIC are provided in DELPHES. Performance parameters for the CLICdet DELPHES cards are taken from studies for CLICdet described and referenced in the following.

2.2.1. Track reconstruction performance

The tracking efficiency is based on studies of the conformal tracking algorithm in [2, Fig. 33 and 35]. Charged hadron efficiencies are based on the results for pions. Efficiencies for muon tracks, electron tracks, and charged hadron tracks are provided as a function of energy and pseudorapidity. In addition, the momentum resolution from tracking is applied according to a log-normal distribution with the resolution given as $\frac{\Delta p_T}{p_T} = a \oplus b/(p \sin \theta)$ binned in pseudorapidity. The parameters used in the CLICdet cards are derived from [2, Sec. 4.2.1, Fig. 31, 32].

2.2.2. Calorimeter performance

DELPHES takes into account the granularity of the calorimeter in terms of pseudorapidity and azimuthal angle. Based on the geometry of the calorimeters described in [1], the $\Delta\eta$ and $\Delta\phi$ segmentations implemented in the CLICdet cards are listed in Table 1.

The energy resolution in the calorimeters is implemented in the DELPHES cards in terms of absolute value, $\Delta E = \sqrt{n^2 + s^2 E + c^2 E^2}$ with noise term n , stochastic term s , and constant term c . In the CLICdet cards, separate resolution parameters are provided for the inner barrel, barrel, transition region and endcaps based on the results from [2, Fig. 37]. The resolution from neutral kaons is used for the HCAL, while the ECAL resolution is determined from photons.

2.2.3. Isolated leptons and photons

Electron, photon, and muon candidates are selected from Particle Flow objects. Identification efficiencies are then applied to mimic the behavior found in full simulation [24], which includes the effects of track reconstruction and particle flow analysis: for electrons with $E > 3 \text{ GeV}$, muons with $E > 2 \text{ GeV}$, and

Table 1: Calorimeter segmentations based on the CLICdet calorimeter cell sizes converted to $\Delta\phi \times \Delta\eta$.

Part	η_{max}	cell size [mm×mm]	$\Delta\phi[^\circ]$	$\Delta\eta$
ECAL barrel	1.2	5×5	0.2	0.003
ECAL endcaps	2.5	5×5	0.8	0.02
ECAL plug	3.0	5×5	1.0	0.02
HCAL barrel	0.8	30×30	1	0.02
HCAL ring	0.9	30×30	1	0.02
HCAL endcaps	3.5	30×30	6	0.1

photons with $E > 2 \text{ GeV}$, the identification efficiencies are given as a function of energy and pseudorapidity [2, Fig. 38-40].

The isolation of an electron, muon or photon is determined according to the jet content in a cone of $\Delta R = 0.1$ surrounding the object. It is considered as isolated if the ratio of the transverse momentum sum of the cone to the transverse momentum of the isolated object does not exceed 0.2. These settings are adapted from isolation criteria used in various full-simulation studies with CLIC detector concepts, e.g. [25].

2.2.4. Heavy flavour tagging

Three working points for tagging of b jets with efficiencies of 50 %, 70 %, and 90 % are provided in the CLICdet cards. The corresponding mis-tagging efficiencies for light flavour and charm jets are extracted from the double spiral option of the vertex endcaps in [26] in bins of pseudorapidity and energy.

The c -tagging performance of CLICdet described in [2, Sec.4.2.6] has not been implemented yet in the CLICdet DELPHES cards.

2.2.5. Tau lepton tagging

The τ tagging efficiencies for the CLIC TauFinder algorithm have been studied in [27]. The CLICdet DELPHES cards use efficiencies averaged for the three processes studied there, resulting in the efficiencies reported in Table 2. Jets are tagged as τ jets according to these efficiencies, using a mis-identification rate of 3 %. As the TauFinder uses a relatively simple, cut-based approach it is expected that its performance can be significantly improved with respect to these numbers by introducing a multivariate analysis.

Table 2: Efficiencies of the TauFinder for linear collider detectors adapted from [27].

$p_T(\tau)$ [GeV]	≥ 5	≥ 12.5	≥ 25	≥ 50	≥ 75	≥ 125	≥ 250
ε	0.84	0.79	0.74	0.66	0.61	0.51	0.36

2.3. Effect of beam-induced backgrounds

The high bunch charge density at CLIC leads to strong radiation from the incoming beams due to their interaction with the field of the other beam. This results in beam-induced background processes, e.g. $\gamma\gamma \rightarrow \text{hadrons}$. To account for its effects, a jet energy smearing is applied. It should be noted that the current implementation of the jet energy smearing assumes massless jets.

In the reconstruction, timing information of the energy deposits in the detector is used to reduce the impact of the $\gamma\gamma \rightarrow$ hadrons background. At the 380 GeV energy stage, this allows almost complete mitigation of the effect [28]. At the higher energy stages, some impact remains despite the timing cuts. It is mimicked by applying an additional smearing of the jet energy. The impact of $\gamma\gamma \rightarrow$ hadrons background on the jet energy resolution depends on the centre-of-mass energy, being most severe at $\sqrt{s} = 3$ TeV at CLIC. Therefore, separate cards are supplied for the three stages of CLIC, as given in Appendix A. For the energy stage at $\sqrt{s} \approx 380$ GeV, denoted as Stage 1, no jet energy smearing is applied. The jet energy is smeared according to the corresponding resolutions at Stages 2 ($\sqrt{s} \approx 1.5$ TeV) and 3 ($\sqrt{s} \approx 3$ TeV).

3. Fast simulation and reconstruction

3.1. Application chain

The various components (DELPHES modules) are called in the CLICdet card in the following order: Particles are propagated through the magnetic field of 4 T with the `ParticlePropagator` module. In the next step, charged hadrons, electrons, and muons are retained or rejected based on random numbers drawn according to the tracking efficiencies. Their momenta are then smeared according to the corresponding momentum resolutions. The tracking efficiencies as well as the momentum resolutions are given as a function of pseudorapidity and transverse momentum, see Sec. 2.2.1. Energy deposits in the electromagnetic and hadronic calorimeters are then generated from the given expected energy fractions, taking into account the granularity of the calorimeter towers and the resolutions described in Sec. 2.2.2. A particle flow algorithm is applied to the tracks and calorimeter deposits using the `EFlowMerger` module. Next, photon, charged hadron, electron, and muon reconstruction efficiencies and isolation efficiencies are applied according to Sec. 2.2.3. To prepare for the jet clustering, isolated electrons, muons, and photons are removed from the list of objects passed to the jet finder using an `EFlowFilter` module. Jet clustering with the VLC algorithm is applied to the remaining objects as described in Sec. 3.2. In the CLICdet DELPHES cards for the higher energy stages (Stages 2 and 3, $\sqrt{s} > 1$ TeV), the effect of $\gamma\gamma \rightarrow$ hadrons background is mimicked by applying a `JetMomentumSmearing` module (see Sec. 2.3). Finally, the `JetFlavorAssociation`, `BTagging` and `TauTagging` modules are run to first find the true flavour of the jet and then to apply tagging efficiencies as well as mis-tagging efficiencies for b -jets and hadronic τ candidates. Three working points for b tagging with tagging efficiencies of 50 %, 70 %, and 90 % are provided in bins of pseudorapidity and energy (Sec. 2.2.4). Tagging efficiencies for hadronic τ s are provided in bins of transverse momentum (Sec. 2.2.5).

3.2. Linear collider jet clustering

Due to the lower levels of background at lepton colliders, rather large cone size parameters R can be used for jet clustering compared to typical values at hadron colliders, leading to better mass resolutions for hadronic resonances.

However, using larger R implies that the jets can have a substructure of smaller R jets. At analysis level, this is usually crucial information, e.g. for suppression of backgrounds with a different jet multiplicity or in order to use the correct objects for invariant masses. Therefore, jet clustering is often run in "exclusive mode" [29] as implemented in Fastjet [30, Sec. 3.3.2], with a fixed number of jets. This forces the algorithm to stop when a certain number of jets has been clustered, thus revealing the substructure information directly.

A suitable jet clustering algorithm for high-energy lepton collisions is the Valencia Linear Collider (VLC) algorithm [31, 32]. It is a sequential recombination algorithm adapted to the linear collider environment.

The VLC algorithm as implemented in FastJet-contribs [33], the functionalities for exclusive jet clustering, and the related observables have been added to the DELPHES framework as part of this

work. In the CLICdet cards, the VLC is applied with $\beta = \gamma = 1.0$ and for all combinations of $R = 0.5, 0.7, 1.0, 1.2, 1.5$ and exclusive number of jets $N = 2, 3, 4, 5, 6$ in order to accommodate a range of jet multiplicities that might be useful for the analyses conducted with these cards. A large value of R should be chosen for the first centre-of-mass stage of CLIC and slightly smaller R for higher centre-of-mass due to higher levels of beam-induced background.

4. Validation of the DELPHES simulation

The performance of the DELPHES cards is validated for the three energy stages of CLIC separately by comparing various kinematic observables in important physics processes obtained with the corresponding CLICdet DELPHES card with full simulation based on the CLIC_ILD, CLIC_SiD, and CLICdet models.

Studies in the CDR [12] use the CLIC_ILD and CLIC_SiD models. Therefore, large event samples are available for these models and hence part of the validation uses CLIC_ILD or CLIC_SiD detector simulation. The performance of these detector models is similar to that of CLICdet for the relevant aspects.

The validation is based on the processes summarised in Table 3. For each of the samples, the CLICdet DELPHES card corresponding to the CLIC energy stage has been used, i.e. for Stage N the card named `delphes_card_CLICdet_StageN.tcl`.

Table 3: Overview of the samples used for validation of the CLICdet DELPHES cards.

Process	\sqrt{s} [GeV]	Stage	Detector	Performance of
HZ, Z \rightarrow q \bar{q} , H \rightarrow incl.	350	1	CLIC_o3_v14	jets at low energy and low $\gamma\gamma \rightarrow$ had. background
Hv $\bar{\nu}$, H \rightarrow $\mu\mu$	1400	2	CLIC_ILD	muons; dimuon mass resolution
W ⁺ W ⁻ \rightarrow $\ell\nu q\bar{q}$	3000	3	CLIC_ILD	jets and leptons at high energy and high $\gamma\gamma \rightarrow$ had. background
t \bar{t} H, H \rightarrow b \bar{b} , t \bar{t} \rightarrow semileptonic	1400	2	CLIC_SiD	jets and leptons with $\gamma\gamma \rightarrow$ had. background

4.1. Higgsstrahlung with hadronic Z decay at 350 GeV

The process $e^+e^- \rightarrow Z(\rightarrow q\bar{q})H(\rightarrow \text{incl.})$ is evaluated at $\sqrt{s} = 350$ GeV. This is an important process for the CLIC physics programme as the model-independent measurement of Higgs properties relies on it. It allows the performance of the CLICdet card to be validated for jets at low energy and with low levels of beam-induced $\gamma\gamma \rightarrow$ hadrons background. For the validation, observables obtained by running DELPHES with the CLICdet card of the first stage are compared with full detector simulation for CLICdet, version CLIC_o3_v14. In both cases, the same generator level events produced with WHIZARD interfaced to PYTHIA6 for the parton shower and hadronisation are used. Jets from VLC with $N=4$, $R=1$ and $\beta = \gamma = 1$ are used unless noted otherwise.

Jet observables are shown in Fig. 1. Good agreement at the level of better than 5% is found for central jets over most of the transverse momentum range above 10 GeV. Up to 10% disagreement is found in the forward region $1.5 < |\eta| < 2.5$. Larger disagreements exist only at low transverse momentum $p_T < 10$ GeV and high transverse momentum $p_T > 150$ GeV.

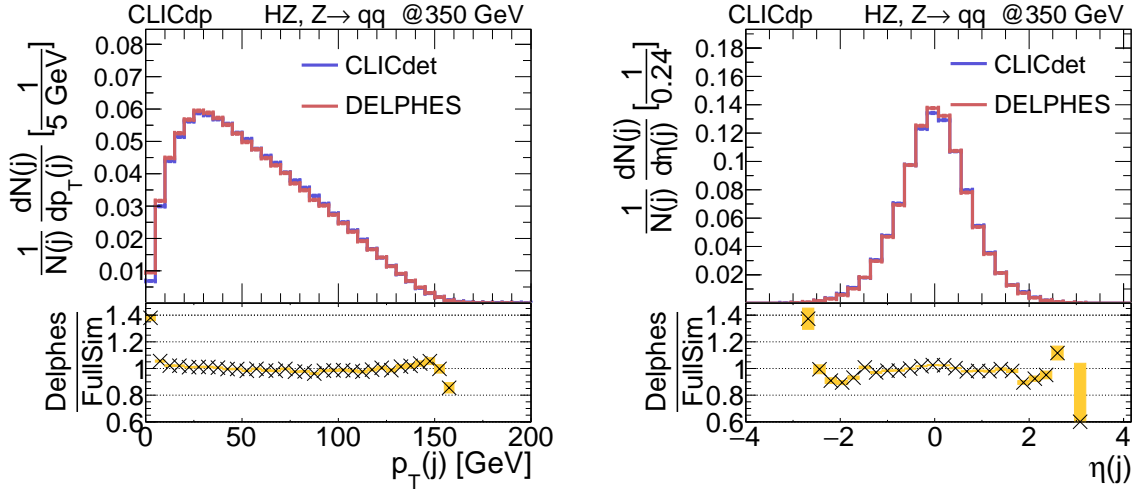


Figure 1: Comparison of jet transverse momentum (left) and pseudorapidity (right) in Higgsstrahlung events with hadronic Z decay for full simulation of CLICdet (blue) and DELPHES (red).

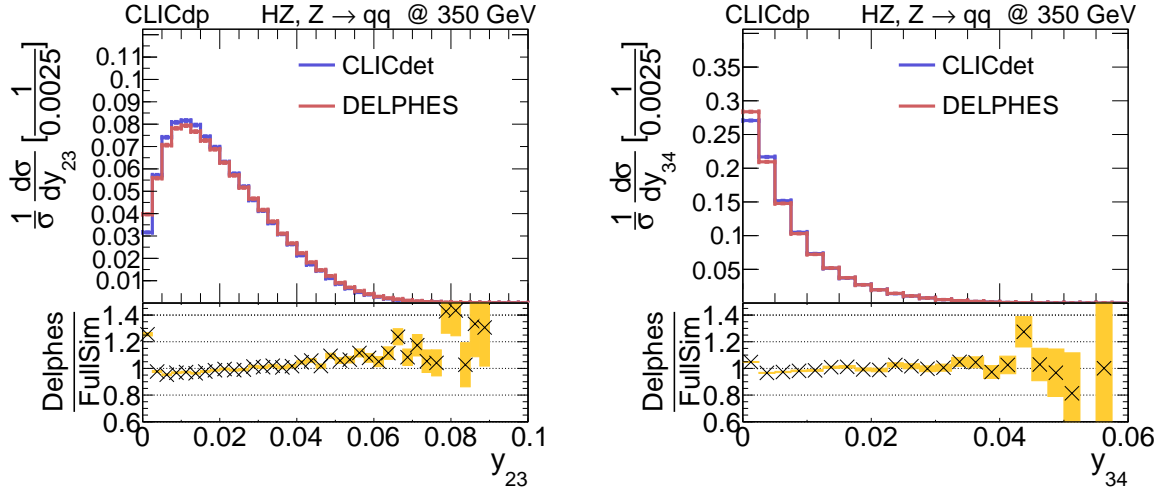


Figure 2: Comparison of jet resolution thresholds y_{23} (left) and y_{34} (right) in Higgsstrahlung events with hadronic Z decay for full simulation of CLICdet (blue) and DELPHES (red).

Jet resolution threshold observables obtained from the exclusive clustering mode are shown in Fig. 2. The variable y_{23} (y_{34}) is the distance measure associated with merging from 3 to 2 (4 to 3) jets [30, Sec. 3.3.2]. They are well-modelled apart from a slight shift to higher values for DELPHES.

The Higgsstrahlung process is further analysed by choosing the configuration of two jets with an invariant mass closest to the mass of the Z boson, m_Z , among the possible combinations obtained by clustering the event with 2, 3, and 5 jets exclusively. Fig. 3 shows the good agreement of the di-jet invariant mass for Z jets (left) and the recoil mass (right) between full simulation and DELPHES. Systematic differences mostly below 10% are seen in the low tail of the invariant mass distribution and in the slopes of the recoil mass. Additional kinematic distributions can be found in Appendix B.1.

4.2. Semi-leptonic top-quark pairs associated with a Higgs boson at 1.4 TeV

The process $e^+e^- \rightarrow t\bar{t}H$ with semi-leptonic decay of the $t\bar{t}$ pair and Higgs decays to $b\bar{b}$ at 1.4 TeV collision energy is simulated with the CLIC_SiD detector model [12], including the beam-induced back-

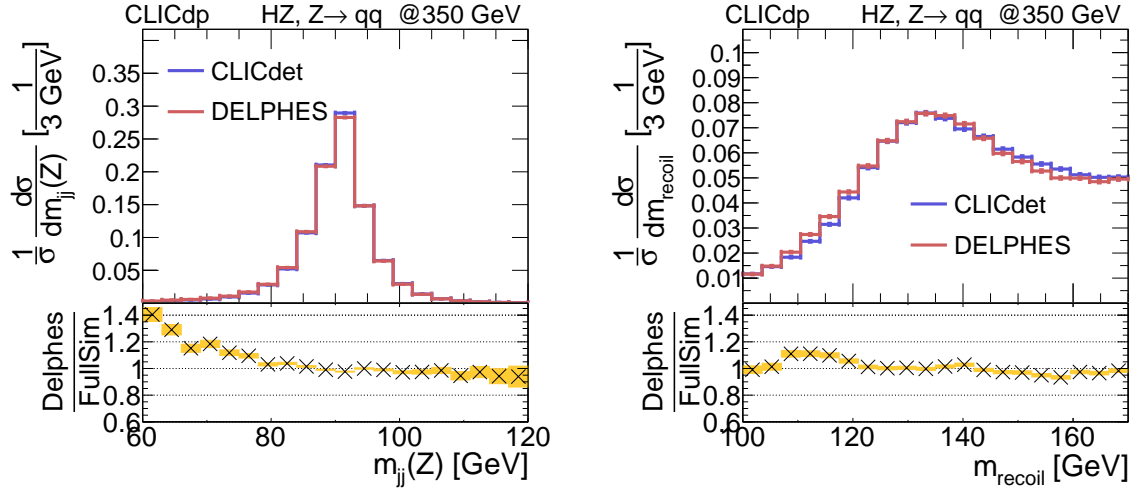


Figure 3: Comparison of the di-jet mass of jets assigned to the Z boson (left) and the recoil mass (right) in Higgsstrahlung events with hadronic Z decay for full simulation of CLICdet (blue) and DELPHES (red).

ground from $\gamma\gamma \rightarrow \text{hadrons}$. Jet clustering is performed with the VLC algorithm with $R = 1.0$ and $N=6$. This process allows validation of the performance of leptons and jets, including the effect of beam-induced background.

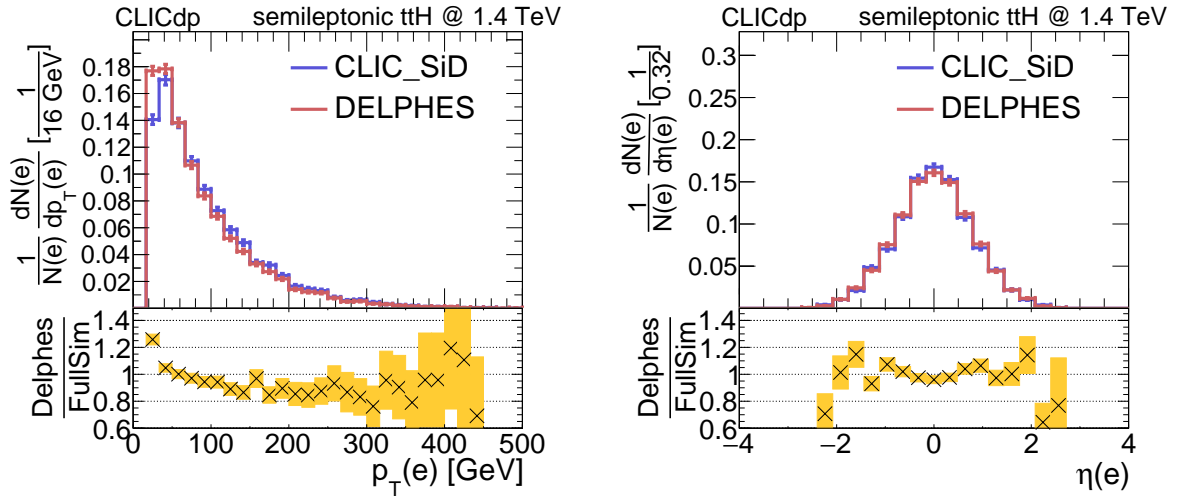


Figure 4: Comparison of electron transverse momentum (left) and pseudorapidity (right) in semileptonic $t\bar{t}H$ events for full simulation of CLIC_SiD (blue) and DELPHES (red).

In the full simulation analysis, optimised isolation criteria are used which give good performance down to low momenta. A cut on the transverse momentum of electrons and muons requiring at least 20 GeV selects the region where the cone-based isolation with a transverse momentum ratio cut as implemented in DELPHES is applicable. The performance of the CLICdet DELPHES card for electrons is demonstrated in Fig. 4. Good agreement can be seen in the transverse momentum of the electron, Fig. 4 (left), with the DELPHES distribution shifted to smaller values of transverse momentum. Fig. 4 (right) shows the pseudorapidity distribution, which is well-modelled. The performance of the fast simulation for muons and jets is presented in Appendix B.2.

4.3. Di-boson production WW at 3 TeV

The performance of fast simulation for muons and jets is validated using the process $e^+e^- \rightarrow \ell\nu q\bar{q}$ at 3 TeV. Jet clustering is performed with the VLC algorithm using $R=0.7$ and $N=2$. Beam induced $\gamma\gamma \rightarrow \text{hadrons}$ background is overlaid in the full simulation, and its effects are taken into account in the fast simulation. Figure 5 demonstrates the validation of the muon simulation. The transverse momentum and pseudorapidity are in agreement between full and fast simulation.

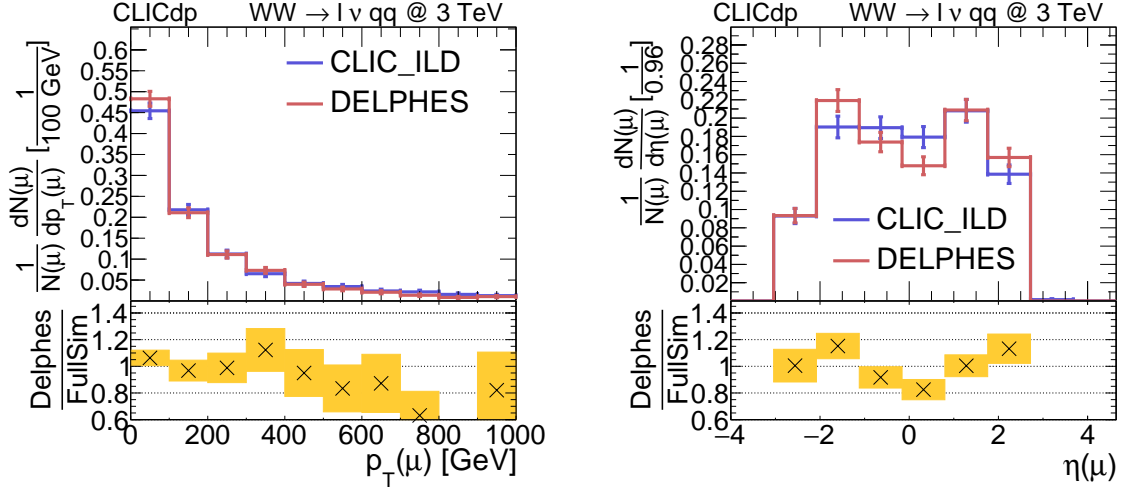


Figure 5: Validation of fast simulation performance for the muon transverse momentum (left) and pseudorapidity (right) for events with the final state $\ell\nu q\bar{q}$ at 3 TeV with full simulation of CLIC_ILD (blue) and fast simulation with DELPHES (red).

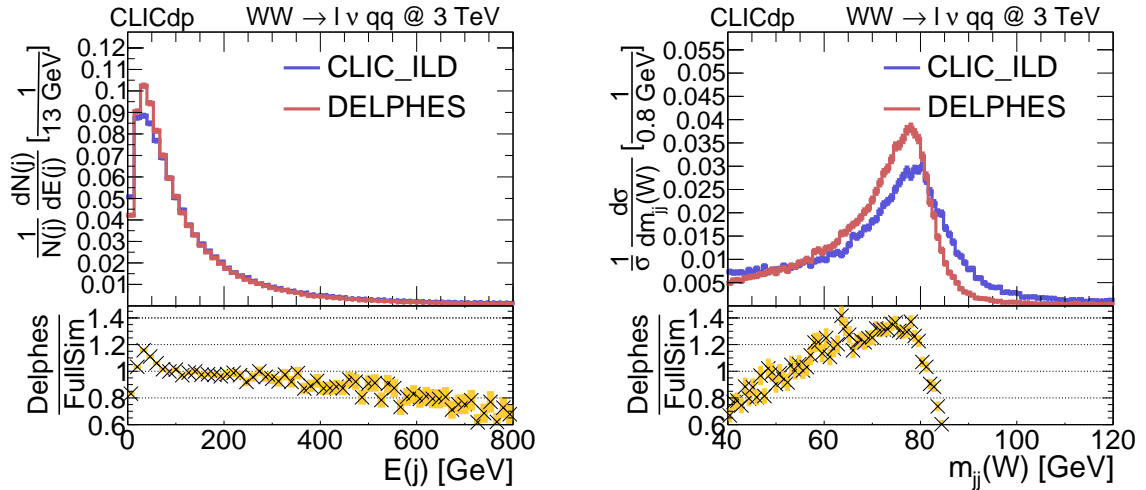


Figure 6: Validation of fast simulation performance for jet energy (left) and di-jet invariant mass (right) using events with the final state $\ell\nu q\bar{q}$ at 3 TeV with full simulation of CLIC_ILD (blue) and fast simulation with DELPHES (red).

The performance of the DELPHES simulation for jets at CLIC is presented in Fig 6. The energy is shifted to lower values for DELPHES. The invariant mass of the two jets, associated with the W boson, is reconstructed with a narrower width and shifted to lower values in DELPHES compared to the full simulation. As the jet clusters all of the typically soft particles from the background distributed within

its entire area, the effect on the mass due to their angular spread is larger than the effect on the energy. The description could be improved by smearing not only the energy but also the mass. Alternatively, one could overlay $\gamma\gamma \rightarrow$ hadrons events. However, highly granular timing information from the detector is crucial to suppress contributions from $\gamma\gamma \rightarrow$ hadrons. The current implementation cannot estimate this suppression and its impact on the reconstruction of the signal process since no timing information is available in the DELPHES simulation.

Additional kinematic distributions of jets can be found in Appendix B.3.

4.4. Di-muon mass resolution in Higgs decays to muon pairs at 350 GeV and 1.4 TeV

The di-muon mass resolution is validated in $H \rightarrow \mu\mu$ decays at 350 GeV and 1.4 TeV. The Higgs boson resonance peaks in the di-muon mass distributions for the two energy stages are shown in Fig. 7. The corresponding mean and width obtained with a Gaussian fit are presented in Table 4. The resulting

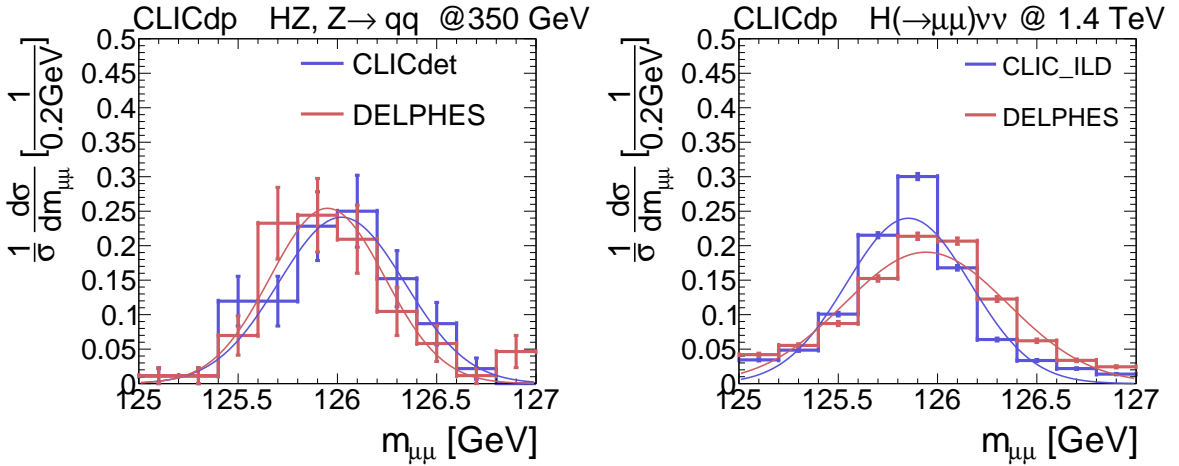


Figure 7: Validation of the di-muon peak obtained in $H \rightarrow \mu\mu$ decays at in HZ events at 350 GeV (left) and in $H\nu\nu$ events at 1.4 TeV (right). Full detector simulation events (blue) are compared with events produced by applying the CLICdet DELPHES card (red).

mean and width of the Gaussian di-muon peak are in good agreement for $H(\rightarrow \mu\mu)Z(\rightarrow q\bar{q})$ events at 350 GeV and in agreement within 30% for $H(\rightarrow \mu\mu)\nu\nu$ events at 1.4 TeV. As shown in [2, Fig. 32], tracking resolutions in the forward region are less well described by the assumed parametrisation than in the central region. As the muons in W-boson fusion $H(\rightarrow \mu\mu)\nu\nu$ events are more forward in the detector than those in $H(\rightarrow \mu\mu)Z(\rightarrow q\bar{q})$ events, this explains the larger discrepancy between DELPHES and full simulation for the di-muon mass in the W-boson fusion $H(\rightarrow \mu\mu)\nu\nu$ process.

Table 4: Resulting parameters of a Gaussian fit to the invariant di-muon mass in $H \rightarrow \mu\mu$ events

Simulation	$H(\rightarrow \mu\mu)Z(\rightarrow q\bar{q})$ at 350 GeV		$H(\rightarrow \mu\mu)\nu\nu$ at 1.4 TeV	
	μ [GeV]	σ [GeV]	μ [GeV]	σ [GeV]
Full detector	126.0 ± 0.03	0.32 ± 0.03	125.8 ± 0.003	0.31 ± 0.003
DELPHES	125.9 ± 0.04	0.29 ± 0.03	125.9 ± 0.004	0.41 ± 0.005

5. Conclusions

Three parameter cards for the detector model for CLIC, CLICdet, have been prepared for the DELPHES framework. They describe the CLICdet geometry and performance for the three energy stages of CLIC. Performance parameters are based on full simulation studies of the detector response and reconstruction software. The cards have been validated by comparing with full simulation for various processes. At the first energy stage of CLIC with low levels of beam-induced background, the validation has found good agreement in particular for single object observables. Also derived observables such as di-jet invariant masses are well described in the regions. At the higher energy stages, reasonable agreement has been found for transverse momentum, energy, and pseudorapidity distributions of leptons and jets. The absence of the beam-induced background in the fast simulation limits the ability to reproduce all observables fully accurately. A smearing of the jet energy has been applied to mimic the effects of $\gamma\gamma \rightarrow$ hadrons background. This could be improved in the future by applying a smearing also to the jet mass.

As DELPHES has so far been used mainly for studies at hadron colliders, some features of detectors at lepton colliders had not yet been implemented. Exclusive jet clustering and the VLC algorithm have been added as part of this study. In addition, implementations for c -tagging and for the very forward calorimeters as well as a refinement of the isolation criteria could be added in the future. The possibility of overlaying beam-induced $\gamma\gamma \rightarrow$ hadrons events would improve the description of detectors at linear colliders. However, this would also require to add the simulation of time information to exploit the timing selection capabilities of the detector to suppress these background contributions.

Full simulation studies for future experiments remain indispensable for the evaluation of the detector performance. Furthermore, they are necessary for analyses using observables that are sensitive to beam-induced backgrounds and rely on timing information, analyses based on tails of distributions that are not well-modelled by fast simulation, as well as analyses using exotic signatures such as long-lived particles.

In conclusion, a good description of the detector concept for CLIC has been achieved in the DELPHES fast simulation framework with the parameter cards discussed in this note. These cards have been validated and have already been used for CLIC physics studies. The implementation makes it possible to take advantage of the flexibility and accessibility of DELPHES for studying many aspects of the CLIC physics potential.

Acknowledgements

We thank Michele Selvaggi for helpful discussions. This work benefited from services provided by the ILC Virtual Organisation, supported by the national resource providers of the EGI Federation. This research was done using resources provided by the Open Science Grid, which is supported by the National Science Foundation and the U.S. Department of Energy's Office of Science.

References

- [1] N. Alipour Tehrani et al., *CLICdet: The post-CDR CLIC detector model*, CLICdp-Note-2017-001, 2017, URL: <https://cds.cern.ch/record/2254048>.
- [2] CLICdp Collaboration, *A detector for CLIC: main parameters and performance*, CLICdp-Note-2018-005, arXiv:1812.07337, 2018, URL: <https://cds.cern.ch/record/2310912>.
- [3] W. Kilian, T. Ohl, J. Reuter, *WHIZARD: Simulating Multi-Particle Processes at LHC and ILC*, Eur. Phys. J. **C71** (2011) 1742, DOI: [10.1140/epjc/s10052-011-1742-y](https://doi.org/10.1140/epjc/s10052-011-1742-y), arXiv: 0708.4233 [hep-ph].

-
- [4] T. Sjostrand, S. Mrenna, P. Z. Skands, *PYTHIA 6.4 Physics and Manual*, JHEP **05** (2006) 026, DOI: [10.1088/1126-6708/2006/05/026](https://doi.org/10.1088/1126-6708/2006/05/026), arXiv: [hep-ph/0603175](https://arxiv.org/abs/hep-ph/0603175) [hep-ph].
- [5] H. Abramowicz et al., *Higgs Physics at the CLIC Electron-Positron Linear Collider*, Eur. Phys. J. C **77** (2016), Comments: 40 pages, 28 figures 475. 40 p, URL: <https://cds.cern.ch/record/2210491>.
- [6] H. Abramowicz et al., CLICdp, *Top-Quark Physics at the CLIC Electron-Positron Linear Collider* (2018), arXiv: [1807.02441](https://arxiv.org/abs/1807.02441) [hep-ex].
- [7] J. de Favereau et al., The DELPHES 3 collaboration, *DELPHES 3: a modular framework for fast simulation of a generic collider experiment*, Journal of High Energy Physics **2014** (2014) 57, ISSN: 1029-8479, DOI: [10.1007/JHEP02\(2014\)057](https://doi.org/10.1007/JHEP02(2014)057), URL: [https://doi.org/10.1007/JHEP02\(2014\)057](https://doi.org/10.1007/JHEP02(2014)057).
- [8] M. Selvaggi, *DELPHES 3: A modular framework for fast-simulation of generic collider experiments*, J. Phys. Conf. Ser. **523** (2014) 012033, DOI: [10.1088/1742-6596/523/1/012033](https://doi.org/10.1088/1742-6596/523/1/012033).
- [9] A. Mertens, *New features in Delphes 3*, J. Phys. Conf. Ser. **608** (2015) 012045, DOI: [10.1088/1742-6596/608/1/012045](https://doi.org/10.1088/1742-6596/608/1/012045).
- [10] J. de Blas et al., *The CLIC Potential for New Physics* (2018), DOI: [10.23731/CYRM-2018-003](https://doi.org/10.23731/CYRM-2018-003), arXiv: [1812.02093](https://arxiv.org/abs/1812.02093) [hep-ph].
- [11] *Github repository of Delphes*, URL: <https://github.com/delphes/delphes>.
- [12] L. Linssen et al., eds., *CLIC Conceptual Design Report: Physics and Detectors at CLIC*, CERN-2012-003, CERN, 2012, arXiv: [1202.5940](https://arxiv.org/abs/1202.5940) [physics.ins-det].
- [13] P. G. Roloff, A. Robson, *Updated CLIC luminosity staging baseline and Higgs coupling prospects* (2018), URL: <https://cds.cern.ch/record/2645352>.
- [14] M. Frank et al., *DD4hep: A Detector Description Toolkit for High Energy Physics Experiments*, Journal of Physics: Conference Series **513** (2014) 022010, DOI: [10.1088/1742-6596/513/2/022010](https://doi.org/10.1088/1742-6596/513/2/022010), URL: <https://doi.org/10.1088/1742-6596/513/2/022010>.
- [15] S. Agostinelli et al., *Geant4 – a simulation toolkit*, Nuclear Instruments and Methods in Physics Research Section A: Accelerators, Spectrometers, Detectors and Associated Equipment **506** (2003) 250, ISSN: 0168-9002, DOI: [https://doi.org/10.1016/S0168-9002\(03\)01368-8](https://doi.org/10.1016/S0168-9002(03)01368-8), URL: <http://www.sciencedirect.com/science/article/pii/S0168900203013688>.
- [16] J. Allison et al., *Geant4 developments and applications*, IEEE Transactions on Nuclear Science **53** (2006) 270, ISSN: 0018-9499, DOI: [10.1109/TNS.2006.869826](https://doi.org/10.1109/TNS.2006.869826).
- [17] J. Allison et al., *Recent developments in Geant4*, Nuclear Instruments and Methods in Physics Research Section A: Accelerators, Spectrometers, Detectors and Associated Equipment **835** (2016) 186, ISSN: 0168-9002, DOI: [10.1016/j.nima.2016.06.125](https://doi.org/10.1016/j.nima.2016.06.125), URL: <http://www.sciencedirect.com/science/article/pii/S0168900216306957>.
- [18] F. Gaede, *Marlin and LCCD: Software tools for the ILC*, Nucl. Instrum. Meth. **A559** (2006) 177, DOI: [10.1016/j.nima.2005.11.138](https://doi.org/10.1016/j.nima.2005.11.138).

-
- [19] E. Brondolin et al., *Conformal Tracking for all-silicon trackers at future electron-positron colliders*, tech. rep. CLICdp-Pub-2019-003, Geneva: CERN, 2019, URL: <https://cds.cern.ch/record/2684496>.
- [20] M.A. Thomson, *Particle flow calorimetry and the PandoraPFA algorithm*, Nuclear Instruments and Methods in Physics Research Section A: Accelerators, Spectrometers, Detectors and Associated Equipment **611** (2009) 25, ISSN: 0168-9002, DOI: 10.1016/j.nima.2009.09.009, URL: <http://www.sciencedirect.com/science/article/pii/S0168900209017264>.
- [21] J. S. Marshall, A. Münnich, M. A. Thomson, *Performance of Particle Flow Calorimetry at CLIC*, Nucl. Instrum. Meth. **A700** (2013) 153, DOI: 10.1016/j.nima.2012.10.038, arXiv: 1209.4039 [physics.ins-det].
- [22] J. S. Marshall, M. A. Thomson, *The Pandora Software Development Kit for Pattern Recognition*, Eur. Phys. J. **C75** (2015) 439, DOI: 10.1140/epjc/s10052-015-3659-3, arXiv: 1506.05348 [physics.data-an].
- [23] T. Suehara, T. Tanabe, *LCFIPlus: A Framework for Jet Analysis in Linear Collider Studies*, Nucl. Instrum. Meth. **A808** (2016) 109, DOI: 10.1016/j.nima.2015.11.054, arXiv: 1506.08371 [physics.ins-det].
- [24] M. A. Weber, *Jet Performance at CLIC*, CLICdp-Note-2018-004, 2018, URL: <https://cds.cern.ch/record/2648827>.
- [25] S. Redford, P. Roloff, M. Vogel, *Physics potential of the top Yukawa coupling measurement at a 1.4 TeV Compact Linear Collider using the CLIC SiD detector*, CLICdp-Note 2014-001, CERN, 2014.
- [26] N. Alipour Tehrani, P. Roloff, *Optimisation Studies for the CLIC Vertex-Detector Geometry*, CLICdp-Note-2014-002, 2014, URL: <http://cds.cern.ch/record/1742993>.
- [27] A. Münnich, *TauFinder: A Reconstruction Algorithm for τ Leptons at Linear Colliders*, LCD-Note-2010-009, 2010, URL: <https://cds.cern.ch/record/1443551>.
- [28] E. Brondolin, A. Sailer, *Optimization of timing selections at 380 GeV CLIC*, tech. rep. arXiv:1811.00466, Geneva: CERN, 2018, URL: <https://cds.cern.ch/record/2645355>.
- [29] S. Catani et al., *Longitudinally invariant K_t clustering algorithms for hadron hadron collisions*, Nucl. Phys. **B406** (1993) 187, DOI: 10.1016/0550-3213(93)90166-M.
- [30] M. Cacciari, G. P. Salam, G. Soyez, *FastJet User Manual*, Eur. Phys. J. **C72** (2012) 1896, DOI: 10.1140/epjc/s10052-012-1896-2, arXiv: 1111.6097 [hep-ph].
- [31] M. Boronat et al., *A robust jet reconstruction algorithm for high-energy lepton colliders*, Phys. Lett. **B750** (2015) 95, DOI: 10.1016/j.physletb.2015.08.055, arXiv: 1404.4294 [hep-ex].
- [32] M. Boronat et al., *Jet reconstruction at high-energy electron-positron colliders*, Eur. Phys. J. **C78** (2018) 144, DOI: 10.1140/epjc/s10052-018-5594-6, arXiv: 1607.05039 [hep-ex].
- [33] *FastJet contribs*, URL: <https://fastjet.hepforge.org/contrib/>.

A. Instructions for using the CLICdet DELPHES cards

There are three cards for the three energy stages of CLIC. The user chooses the one appropriate for the relevant energy stage as indicated in Table 5. To understand the output of running the card, the b -tagging

Table 5: CLIC energy stages implemented in separate CLICdet DELPHES cards.

Stage	Energy options	Card
Stage1	380 (350) GeV	delphes_card_CLICdet_Stage1.tcl
Stage2	1.5 (1.4) TeV	delphes_card_CLICdet_Stage2.tcl
Stage3	3 TeV	delphes_card_CLICdet_Stage3.tcl

and the correct choice of jet branches is described below.

A.1. B-Tagging in the CLICdet DELPHES card

B-tagging is implemented in the card with three working points (WP), which tag 50%, 70%, and 90% of all b -quark-initiated jets, respectively. The corresponding mis-tagging rates are implemented in the CLICdet card. DELPHES uses a three-bit mask to store the b -tagging information in the following way, where

- bit 0 is the tight WP with 50% b -tagging efficiency,
- bit 1 is the medium WP with 70% b -tagging efficiency,
- bit 2 is the loose WP with 90% b -tagging efficiency.

This leads to the combinations indicated in Table 6. Loosely b -tagged jets are selected with $B_{\text{Tag}} \geq 4$;

Table 6: B-tagging working points in bit-wise code with T for true and F for false.

BTag value	7	6	5	4	3	2	1	0
BTag binary	111	110	101	100	011	010	001	000
(bit 0) & BTag	T	F	T	F	T	F	T	F
(bit 1) & BTag	T	T	F	F	T	T	F	F
(bit 2) & BTag	T	T	T	T	F	F	F	F

for medium b -tagged jets, B_{Tag} should be 2, 3, 6, or 7, and for the tight WP the B_{Tag} should be 1, 3, 5 or 7.

A.2. Taking into account the effect of beam-induced background

The levels of beam-induced $\gamma\gamma \rightarrow$ hadrons events are higher at the high energy stages. To account for their effects, a jet energy smearing is applied in the two cards for Stage2 and Stage3.

The branches with the jet energy smearing applied are then named **JER_VLCjetR(r)N(njets)** in the resulting root file.

B. Supplementary validation studies

B.1. Di-jet mass in Higgsstrahlung with hadronic Z decay at 350 GeV

Using exclusive jet clustering with $N=4$, the Z jets are assigned according to the combination closest to the mass of the Z boson. The invariant mass of the two remaining jets after assigning the Z jets is shown

in Fig. 8(right) as $m_{jj}(\text{H})$.

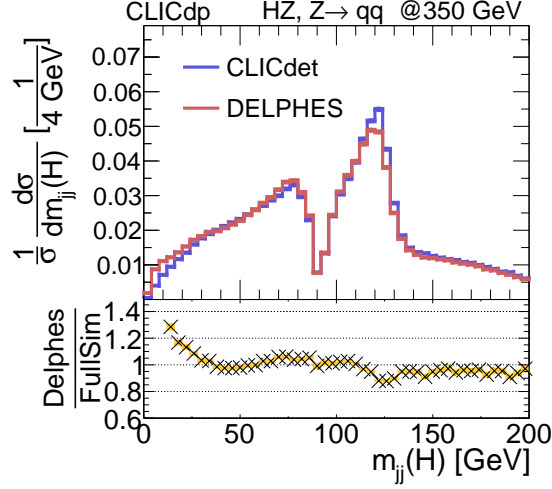


Figure 8: Comparison of the di-jet mass of remaining jets not assigned to the Z boson in Higgsstrahlung events with hadronic Z decay for full simulation of CLICdet (blue) and DELPHES (red).

B.2. Semi-leptonic top-quark pairs associated with a Higgs boson at 1.4 TeV

The fast simulation for muons is validated in Fig. 9. Like for electrons (Fig. 4), the transverse momentum is described reasonably well, but with an increase in contributions from DELPHES at lower values.

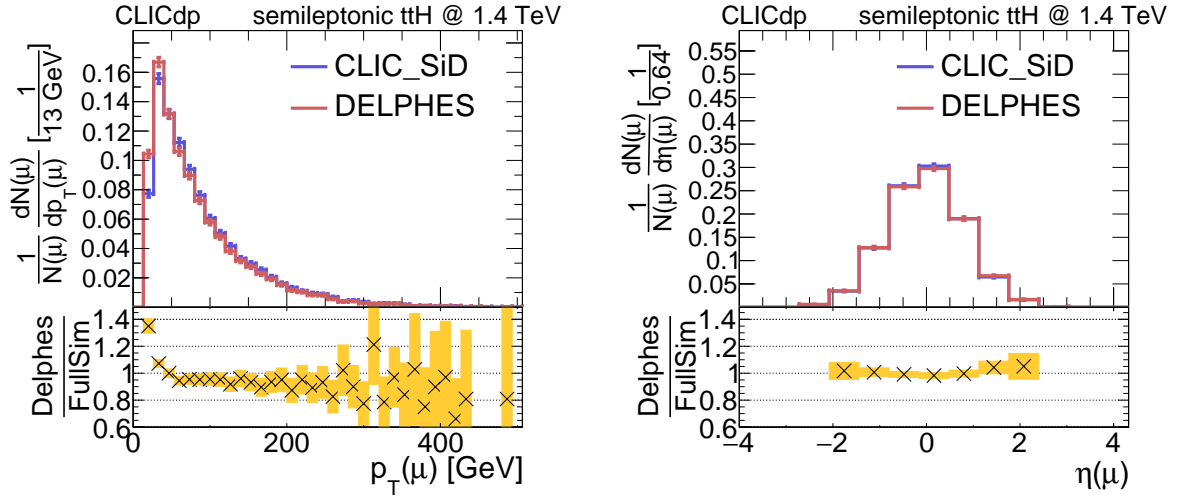


Figure 9: Comparison of muon transverse momentum (left) and pseudorapidity (right) in semileptonic $t\bar{t}H$ events for full simulation of CLIC_SiD (blue) and DELPHES (red).

The jet performance is demonstrated in Fig. 10. It includes the jet energy smearing mimicking the effects of $\gamma\gamma \rightarrow \text{hadrons}$ background. The pseudorapidity distribution is well-modelled, while the DELPHES spectrum for transverse momentum shows an increase of events with low as well as higher transverse momentum.

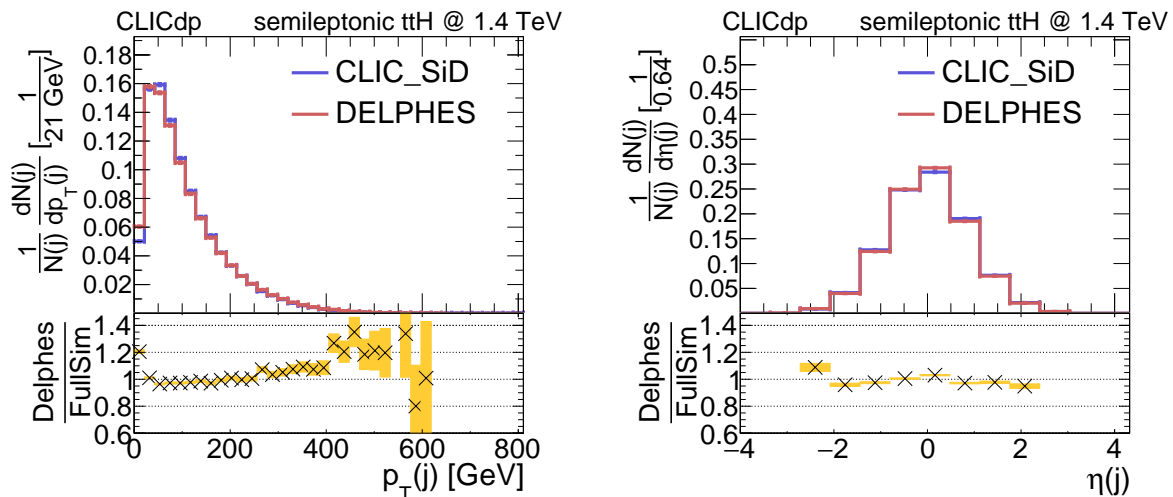


Figure 10: Comparison of jet transverse momentum (left) and pseudorapidity (right) in semileptonic $t\bar{t}H$ events for full simulation of CLIC_SiD (blue) and DELPHES (red).

B.3. Di-boson production WW at 3 TeV

The muon energy distribution is validated comparing DELPHES to full detector simulation with the CLIC_ILD model as shown in Fig. 11.

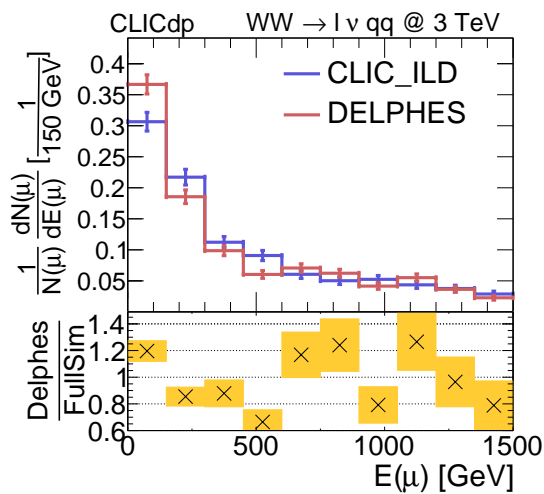


Figure 11: Validation of fast simulation performance for the muon energy for events with the final state $l\nu q\bar{q}$ at 3 TeV with full simulation of CLIC_ILD (blue) and fast simulation with DELPHES (red).

The transverse momentum of the jets is underestimated by the DELPHES simulation, and it does not show all features of the CLIC_ILD detector geometry in the pseudorapidity, as shown in Fig. 12.

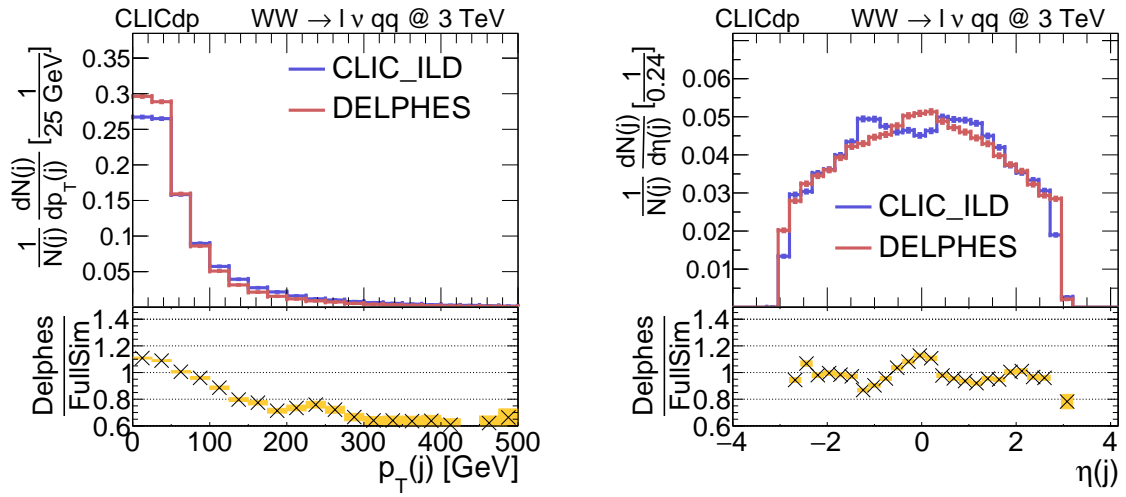


Figure 12: Validation of fast simulation performance for the transverse momentum of jets (left) and the pseudorapidity of jets (right) using events with the final state $\ell \nu q \bar{q}$ at 3 TeV with full simulation of CLIC_ILD (blue) and fast simulation with DELPHES (red).